Online resource for the article submitted to *Climate Dynamics*:

"Analysis of the interannual variability in satellite gravity solutions: detection of climate modes fingerprints in water mass displacements across continents and oceans"

by Julia Pfeffer (1), Anny Cazenave (1, 2), Anne Barnoud (1)

Magellium, 1 rue Ariane, 31520 Ramonville-Saint-Agne, France
LEGOS, Observatoire Midi-Pyrénées, Toulouse, France

Contact author: julia.pfeffer@magellium.fr

COMPARISON OF EMPIRICAL ORTHOGONAL FUNCTIONS OF THE WATER MASS CHANGES OBSERVED DURING THE GRACE AND GRACE-FO MISSIONS WITH CLIMATE INDICES

The principal modes of interannual variability in water mass changes can be explored with EOF (Empirical Orthogonal Functions) analyses carried out on the locally detrended and deseasoned JPL and CSR mascon solutions. Four EOF analyses have been carried out separately for the oceanic and continental domains of the CSR and JPL solutions. Area weighting was taken into account using the cosine of latitude. There was no need to interpolate the CSR and JPL mascon solutions in time as EOF analyses can be carried out on grids irregularly spaced in time. The land-sea mask is derived from the GSHHS (global, self-consistent, hierarchical, high-resolution shoreline database) coastline dataset (Wessel & Smith, 1996) taken at a 1km resolution over a 5 minute spaced grid. Additionally, the regions impacted by the 2004 Sumatra, 2011 Tohoku-Oki and 2010 Chile earthquakes have been masked out. The extent of the regions was set to 13°S to 17°N and 81°E to 111°E for Sumatra, 30°N to 42°N and 132°E to 152°E for Tohoku-Oki and 41°S to 31°S and 277°E to 297°E for Chile according to the analysis by Tang et al. (2020). The masks were applied before the EOF analysis, to focus on interannual water mass displacements, rather than geophysical signals.

1. EOF analyses over the oceans

The leading ocean principal component (PC) (**Fig. OR1**) exhibits a decadal to multidecadal oscillation peaking around 2010 for both solutions (CSR, JPL). A long-period oscillation is detected spanning over the whole the time span of GRACE and GRACE-FO mission. Prominent spatial features include: (i) a negative beak-shaped anomaly across the Southern Pacific and the Southern Ocean, (ii) a positive anomaly in the Southern Ocean beneath the Atlantic and Indian Ocean, (iii) large positive anomalies in shallow seas around Indonesia, the Gulf of Carpentaria and the Mediteranean Sea.

The second ocean PC displays a long-period oscillation with a maximum peaking in 2006 and a minimum around 2016 (**Fig. OR2**). A spectral analysis, carried out with a generalized Lomb-Scargle periodogram (Press & Rybicki, 1989), shows significant power at time scales longer than 10 years for the JPL (**Fig. OR7**). There is also some power at decadal time scales for the CSR, with reduced amplitude in the second PC compared to the third PC (Fig OR7). The second EOF displays large negative anomalies in the tropical Pacific and positive anomalies in the Southern Ocean, Indian Ocean and in the Arctic.

Higher frequencies seem to be present in the third PC (**Fig. OR3**), with several peaks at time scales ranging from a few months to 8 years (**Fig. OR7**). The corresponding EOF shows large positive anomalies in the Southern Ocean and large negative anomalies in the shallow seas around Australia. The JPL also displays a strong negative anomaly across the tropical Pacific.

In summary, the CSR and the JPL display really similar spatial and temporal patterns over the oceanic domain for the three leading PCs and EOFs. For both centers, there is little variability in the Atlantic. As expected from ocean models (Piecuch & Ponte, 2011), a significant part of the ocean-driven variability seems to occur at high latitudes (in the Southern and Arctic Oceans) and around shallow seas (first and third modes of the EOF analysis). Significant ocean mass variability is also observed in the tropical Pacific (second mode of the EOF analysis).

2. EOF analyses over the continents

The leading continental mode (**Fig. OR4**) is extremely similar for the JPL and CSR solutions both for the temporal and spatial components. Similarly to what was shown for the oceans, the leading continental PC exhibits a long-period oscillation peaking in 2011. There is some interannual variability superimposed, anti-correlated with MEI (**Fig. 1** in the main text), as expressed by the decreases occurring in 2009-2011 and 2015-2016, that corresponds to Niño phases, and the increase in 2010-2011, that corresponds to a particularly strong Niña phase. Large positive anomalies are retrieved in the Northeast of South America and central America, across the Okavango river basin (South of African continent), around the Volta lake (West Africa), in the North and Northeast of Australia, in the Penner basin (East India), along the Indus river (Pakistan), along the Mekong river (Thailand) and in the Caspian Sea, in Northeast Europe, punctually over the Winnipeg lake and along the Northwest coast of Canada (**Fig. OR4**). These would be wetter during Niña phases (maxima of the leading PC) and drier during Niño phases (minima of the leading PC). On the opposite, the Parana basin, East coast of the United States, Great Lakes region, Congo basin, Ob and Yenisei basins and Yangtze river exhibit negative anomalies, and would therefore be wetter during the minima of the leading PC (Niño phases) and drier during the maxima of the leading PC (Niña phases) (**Fig. OR4**).

The second continental PC (**Fig. OR5**) remains really similar for the CSR and JPL. The temporal component exhibits a complete oscillation of about 12 to 13 years, with a maximum spanning over the 2005-2009 time period and a minimum spanning from 2013 to 2016. In the second EOFs, both centers exhibit large negative anomalies across the whole Australian continent, in Indonesia and South-East Asia, in the Okavango basin and Victoria lake, along the Parana river and in Europe. These regions would therefore be drier in 2005-2009 and wetter in 2013-2016. Positive anomalies (wetter in 2005-2009 and drier in 2013-2016) are located along the Mississippi river, in the North East of the Amazon basin, at the mouth of the Congo river, along the Tigris and Euphrate rivers, across the Caspian Sea and at the tip of India.

The third continental PC (**Figure OR6**) is again very much alike for the CSR and JPL. The third EOF includes a large negative anomaly covering most of the Amazon basin and several negative anomalies with smaller geographical extent in the north of India, over the Great Lakes, along part of the Mekong, Congo and Zambezi rivers and near the mouth of the Fitzroy river in northwest Australia. Positive anomalies are located over a large part of central and north Australia, along the Parana, in California, along the Rio Grande, in eastern Europe, along the Black Sea, at the tip of India and at the east of China.

3. Periodograms

The spectral content in the three first principal components of locally detrended and deseasoned GRACE and GRACE-FO solutions was calculated using a generalized Lomb Scargle periodogram (e.g. VanderPlas et al., 2012 and 2015; VanderPlas, 2018), commonly used to detect periodic signals in unevenly spaced observations (Press & Rybicki, 1989). The same approach was applied on detrended and deseasoned climate indices selected for the valid months of the GRACE and GRACE-FO missions spanning from April 2002 to July 2020. The spectral content was estimated for monthly spaced periods going from two months to 18 years.

One should be cautious in the interpretation of low frequencies due to the limited time-span of the satellite gravity missions. Usually such tools are used for the interpretation of periods up to half the length of the time series (about 9 years here). The interpretation of power at longer periods should be limited to a qualitative assessment, indicating that there is power at decadal time scales in the time series. The cyclicality could however not be proven by such analysis for periods larger than 9 years and the exact period of the presumed cycles would remain undetermined.

With this warning in mind, we notice that there is redundant evidence of decadal variability in the main components of GRACE/GRACE-FO time series, both over the oceans and the continents (**Fig. OR7**). Such variability could be related to the climate variability, also present in the PDO, ENSO, NPGO, NAO, IOD and SAM (**Fig. OR8**). Because we only consider detrended indices, there is not much power at decadal time scales in the AMO index. The multidecadal oscillations characteristic of this mode were removed with the linear trend and cannot be detected over such a small time period.

There is also some interannual variability evidenced in the GRACE/GRACE-FO PCs, ranging from a few months to 8 years for the oceans (third PC of the JPL and CSR in **Fig. OR7**) and at 5 to 6 years for the continents (third PC of the JPL and CSR in **Fig. OR7**). All the climate indices have complex interannual variability and could explain some degree of variance at these periods (**Fig. OR8**). However, because we are not directly comparing the GRACE time series to climate indices, but only a statistical decomposition of the satellite gravity solutions based on a singular value decomposition, some of the relationships between the satellite gravity measurements and the climate variability could be lost or misrepresented**.** Such relationships would be better investigated through a regression process, improved by a LASSO regularization.

4. Correlations

The Pearson correlation coefficients (R) are computed between the three first oceanic and continental PCs of the locally detrended and deseasoned JPL and CSR solutions and the detrended and deseasoned climate indices (**Fig. OR9**).

Over the oceans (**Fig. OR9**), the most striking correlations are found between the PCs of the CSR and the JPL (R=0.98, 0.71 and 0.75 for the modes 1, 2 and 3 respectively), confirming that the interannual variability extracted with empirical orthogonal functions is very similar in both solutions. The correlations of the ocean PCs with climates indices are rather low, especially when considering AMO, NAO, IOD, AO and SAM. The correlations are a bit stronger with the Pacific modes, namely the PDO, ENSO (characterized with MEI) and NPGO. The first PCs are anticorrelated with the PDO (R=-0.69 and -0.74 for the JPL and CSR respectively) and MEI (R=-0.62 and -0.64 same order) and correlated with the NPGO (R=0.60 and 0.55 same order). All other R values assessing the correlations between the ocean PCs and climate indices are under 0.4.

Part of the GRACE/GRACE-FO-based ocean mass variations are therefore likely to be related with the PDO, ENSO and the NPGO. On the other hand, it does not prove that there are no connections with AMO, NAO, AO or SAM. Several limits in our approach could explain the lack of correlations. First, the EOF analysis was carried out over the global ocean, while climate modes are defined regionally. Besides, we did not directly compare the ocean mass variations to the climate modes, but we compared the results of a singular value decomposition to climate indices. If AMO, NAO, AO or SAM have an influence on the interannual variability of the ocean mass, it may have been pulled apart in several EOF components.

Similar conclusions can be drawn for the continents (**Fig. OR9**), with really high correlations (R>0.98) between the CSR and JPL. Over the continents, the PDO is mildly anticorrelated with the first PCs of the JPL(R=-0.61) and CSR (R=-0.61). MEI is also anticorrelated with the first PCs of the JPL(R=-0.56) and CSR (R=-0.55). NPGO is correlated to the PC1 of the JPL (R=0.51) and CSR (R=0.49). There is also a mild correlation (R = 0.48) between AMO and the third continental PC for the JPL and the CSR. All other R values are under 0.4. This tends to show that there is a mild relationship between the interannual variability of land water resources and climate modes (especially the PDO, ENSO and NPGO). While significant correlations could not be detected with the other modes (AMO, NAO, AO, SAM and IOD), it does not eliminate the possibility of a relationship, but rather stresses the limits of the method, carried out globally (while modes are defined regionally) and on the results of a decomposition that may redistribute physically consistent signals in different EOF components.

List of figures in the online ressource

Figure OR1: Leading PCs and EOFs of locally detrended and deseasoned CSR and JPL mascon solutions over the oceanic domain

Figure OR2: Second PCs and EOFs of locally detrended and deseasoned CSR and JPL mascon solutions over the oceanic domain

Figure OR3: Third PCs and EOFs of locally detrended and deseasoned CSR and JPL mascon solutions over the oceanic domain

Figure OR4: Leading PCs and EOFs of locally detrended and deseasoned CSR and JPL mascon solutions over the continental domain

Figure OR5: Second PCs and EOFs of locally detrended and deseasoned CSR and JPL mascon solutions over the continental domain

Figure OR6: Third PCs and EOFs of locally detrended and deseasoned CSR and JPL mascon solutions over the continental domain

Figure OR7: Periodograms of the three first PCs of the locally detrended and deseasoned JPL, and CSR solutions over the oceans and continents for April 2002 - July 2020

Figure OR8: Periodograms of detrended and deseasoned climate indices calculated for April 2002 - July 2020

Figure OR9: Pearson correlation coefficients between the principal components of interannual water mass changes retrieved with GRACE and GRACE FO measurements and major climate indices.

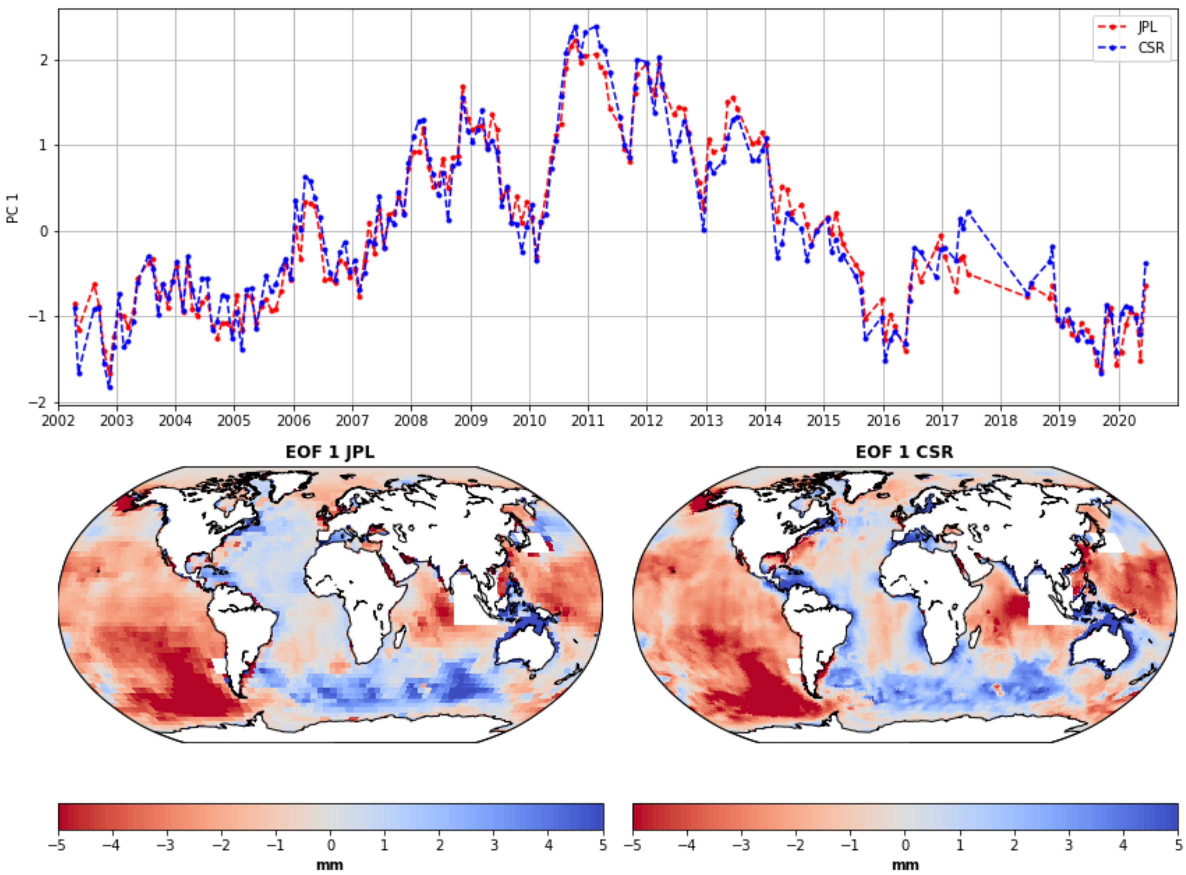

Figure OR1: Leading PCs and EOFs of locally detrended and deseasoned CSR and JPL mascon solutions over the oceanic domain. The regions impacted by the Sumatra, Tohoku-Oki and Chile earthquakes have been masked out according to Tang et al., (2020).

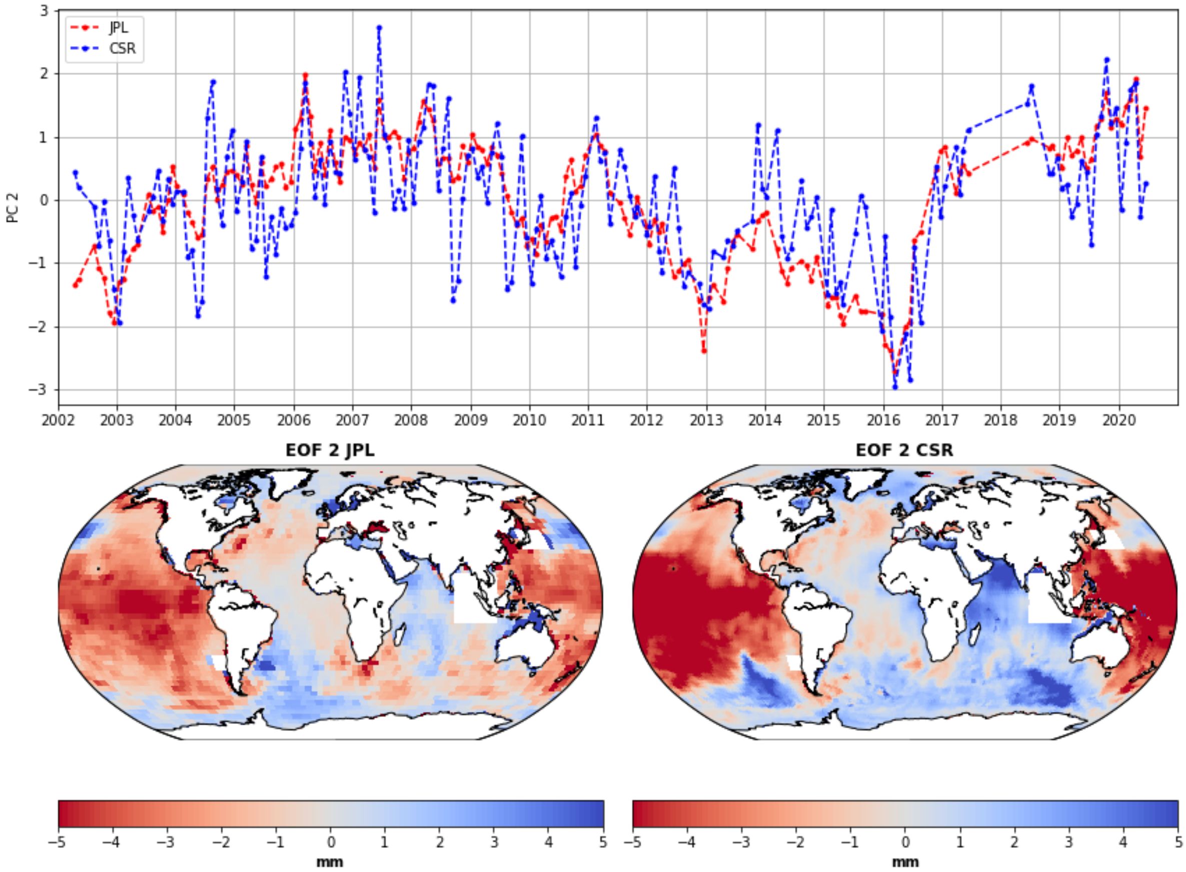

Figure OR2: Second PCs and EOFs of locally detrended and deseasoned CSR and JPL mascon solutions over the oceanic domain. The regions impacted by the Sumatra, Tohoku-Oki and Chile earthquakes have been masked out according to Tang et al., (2020).

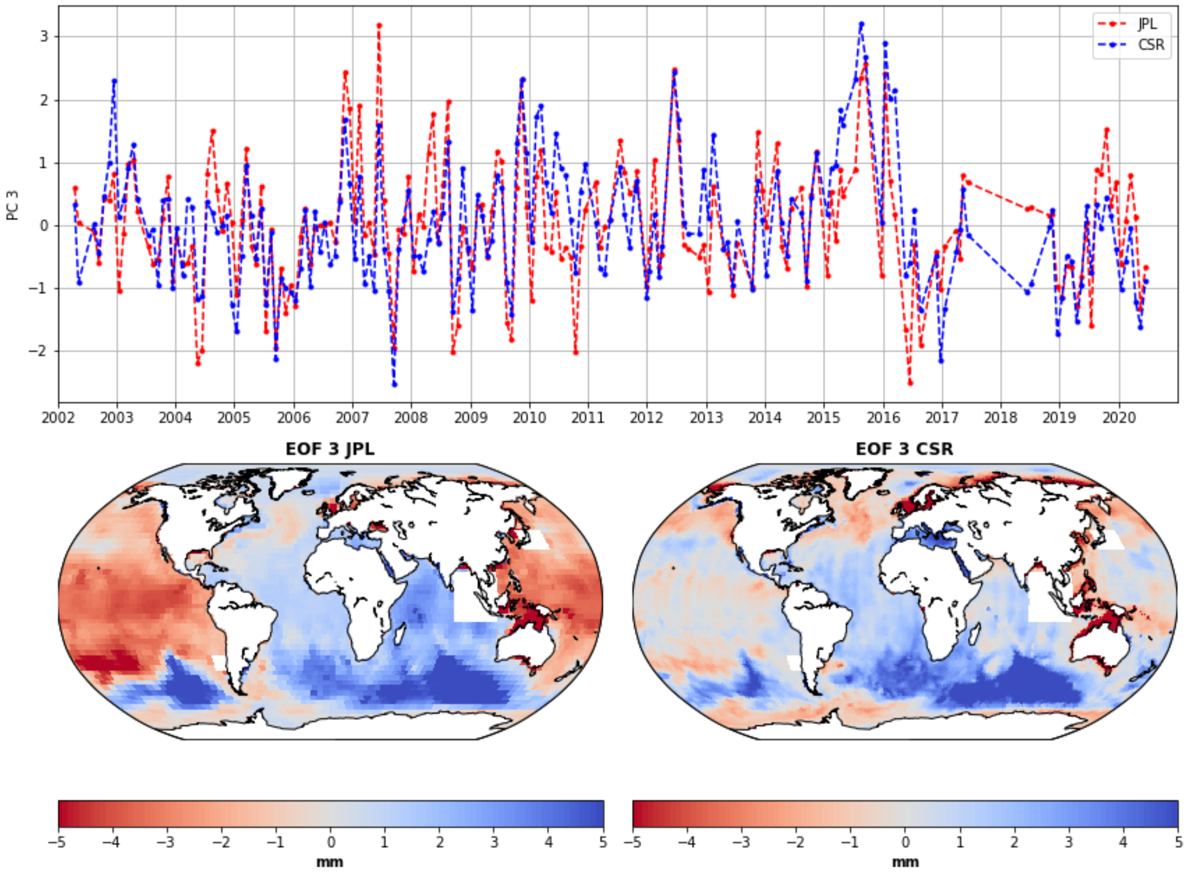

Figure OR3: Third PCs and EOFs of locally detrended and deseasoned CSR and JPL mascon solutions over the oceanic domain. The regions impacted by the Sumatra, Tohoku-Oki and Chile earthquakes have been masked out according to Tang et al., (2020).

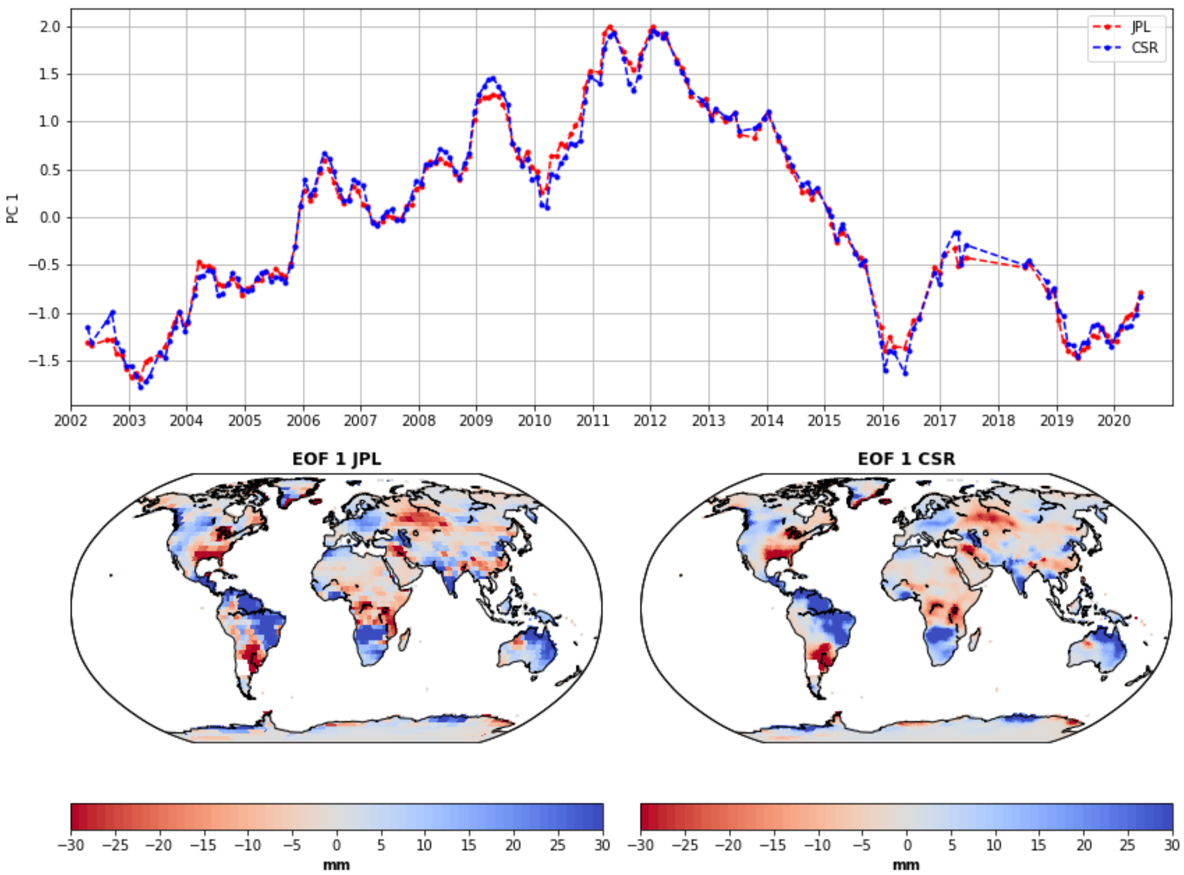

Figure OR4: Leading PCs and EOFs of locally detrended and deseasoned CSR and JPL mascon solutions over the continental domain. The regions impacted by the Sumatra, Tohoku-Oki and Chile earthquakes have been masked out according to Tang et al., (2020).

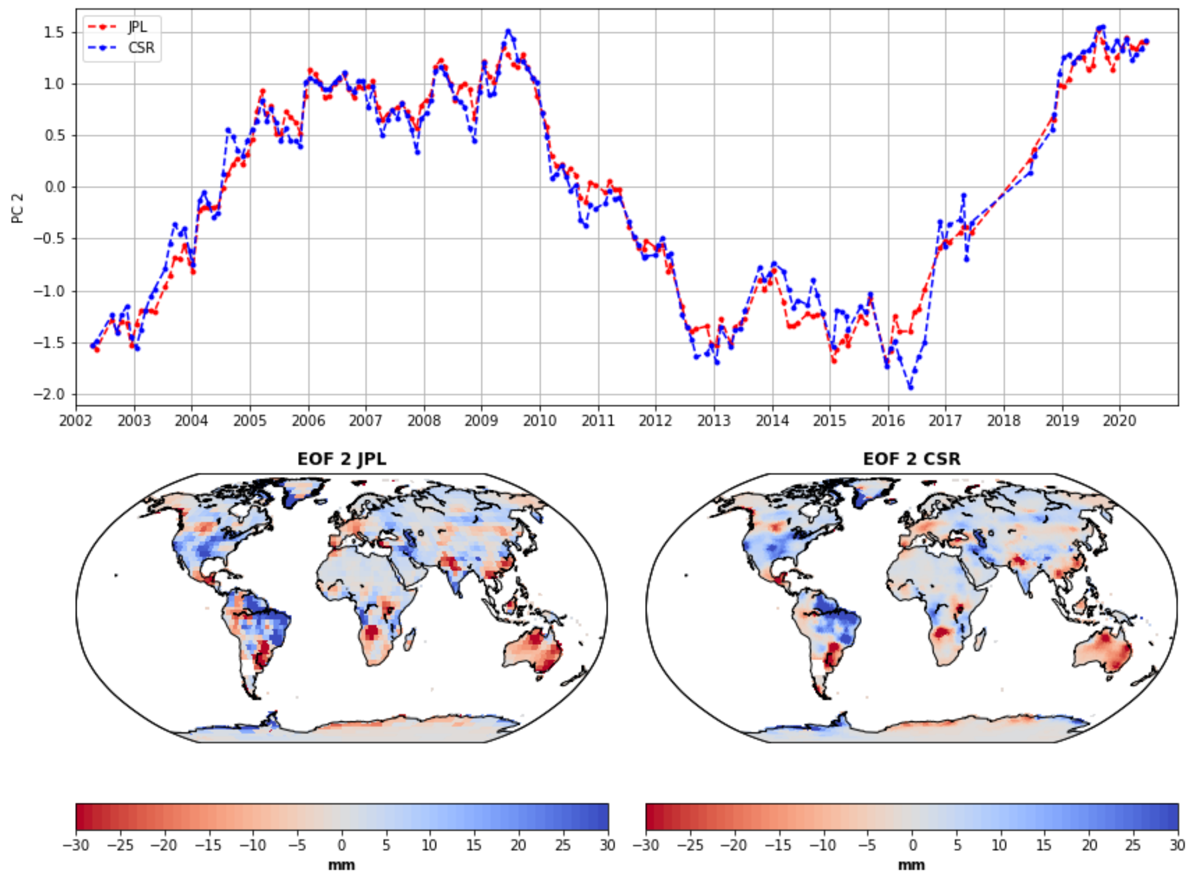

Figure OR5: Second PCs and EOFs of locally detrended and deseasoned CSR and JPL mascon solutions over the continental domain. The regions impacted by the Sumatra, Tohoku-Oki and Chile earthquakes have been masked out according to Tang et al., (2020).

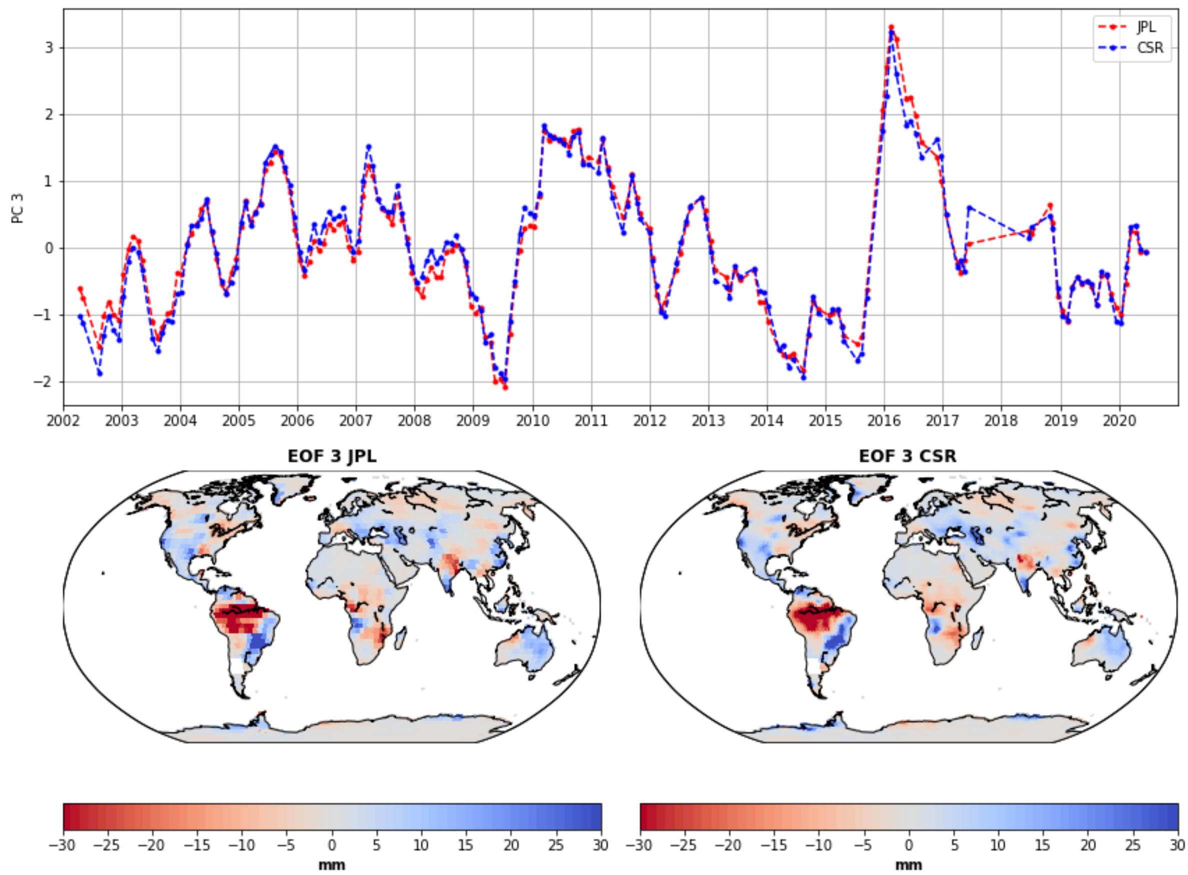

Figure OR6: Third PCs and EOFs of locally detrended and deseasoned CSR and JPL mascon solutions over the continental domain. The regions impacted by the Sumatra, Tohoku-Oki and Chile earthquakes have been masked out according to Tang et al., (2020).

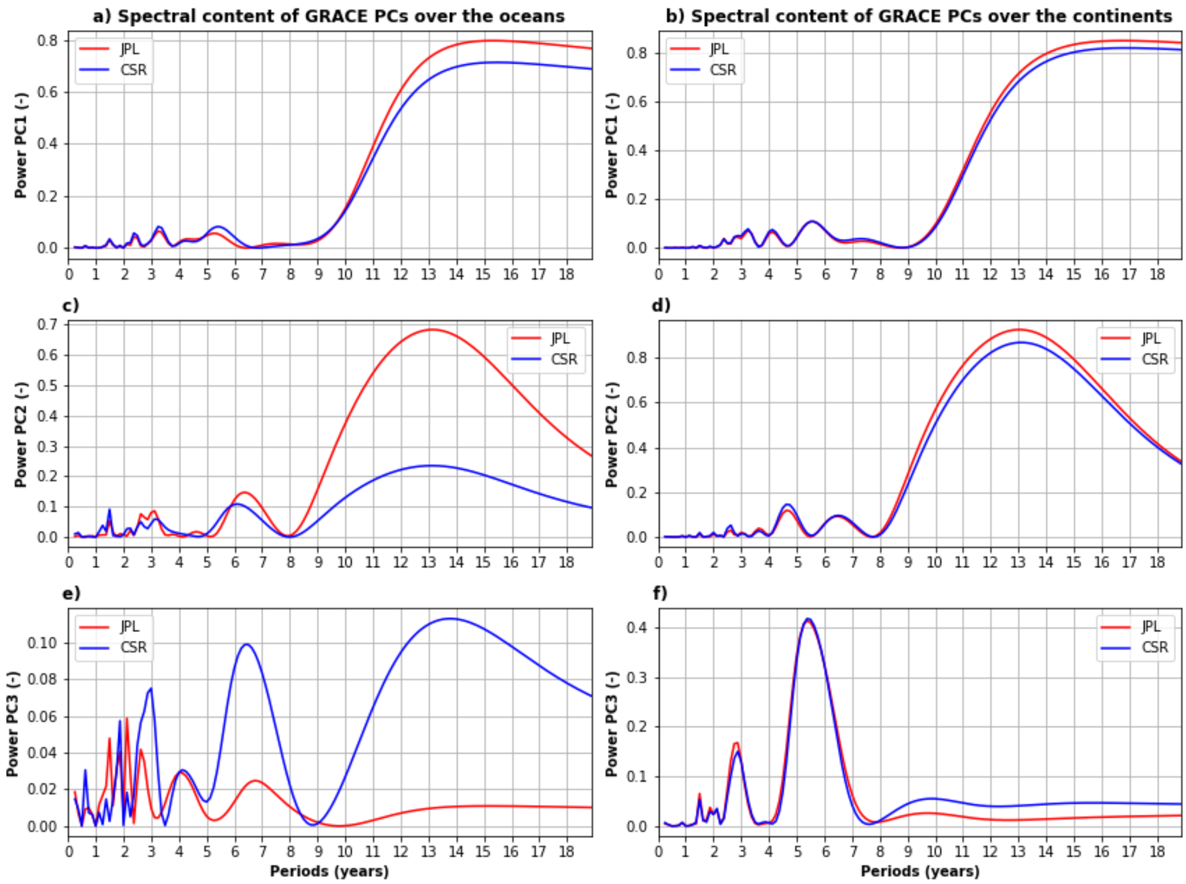

Figure OR7: Periodograms of the three first PCs of the locally detrended and deseasoned JPL, and CSR solutions over the oceans and continents for April 2002 - July 2020.

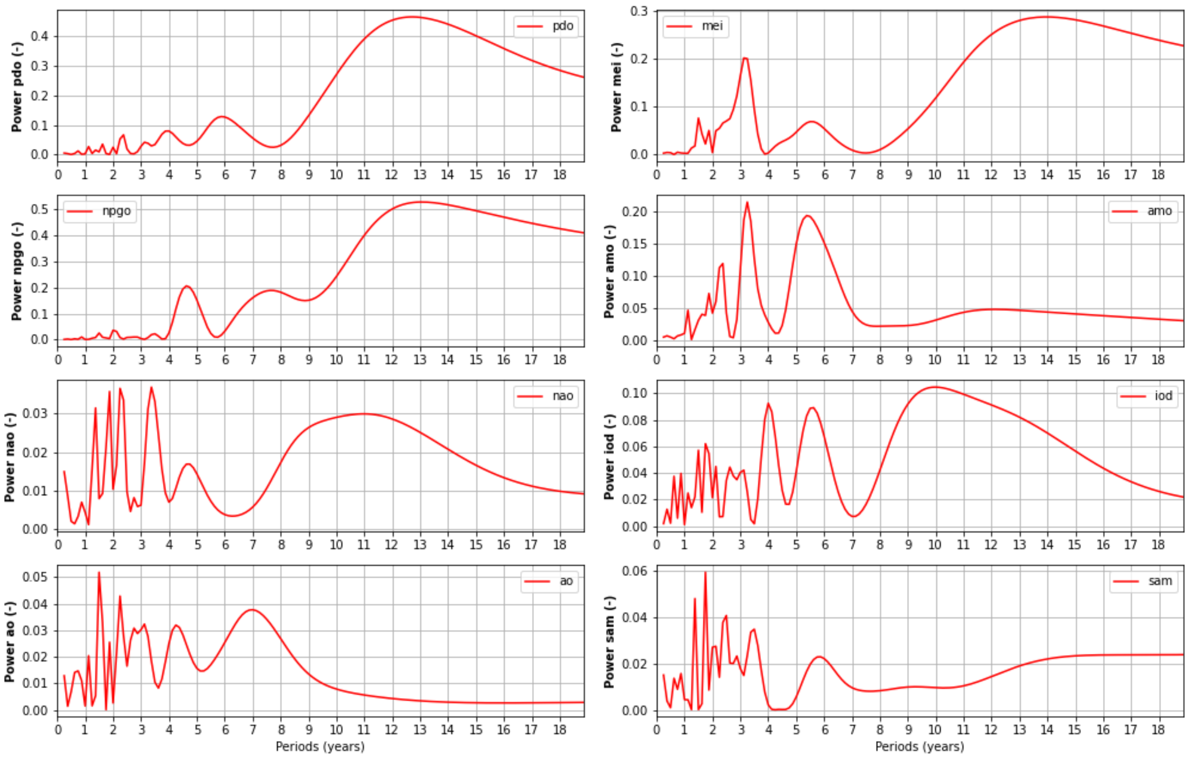

Figure OR8: Periodograms of detrended and deseasoned climate indices calculated for April 2002 - July 2020.

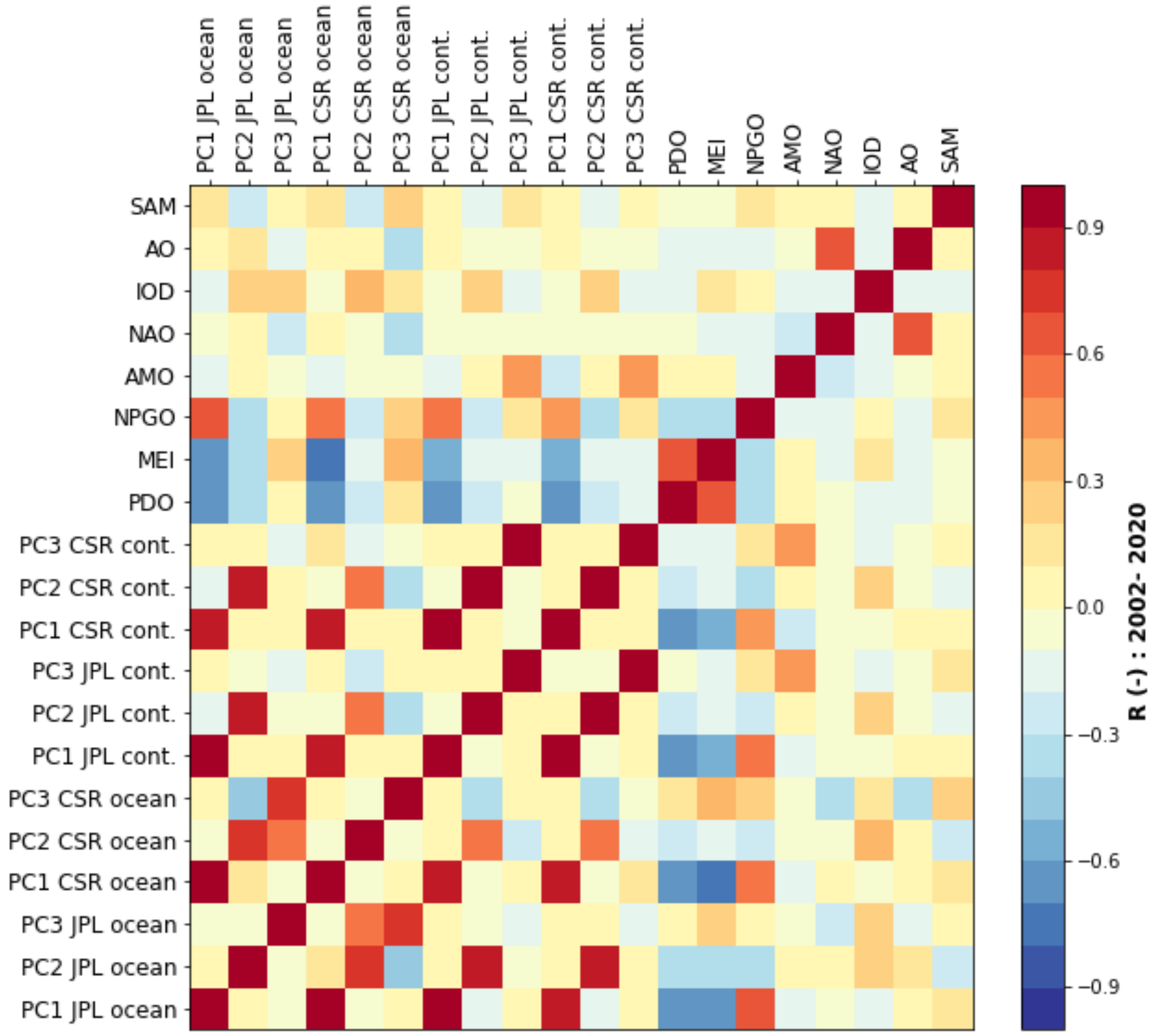

Figure OR9: Pearson correlation coefficients between the principal components of interannual water mass changes retrieved with GRACE and GRACE-FO measurements and major climate indices. The regions impacted by the Sumatra, Tohoku-Oki and Chile earthquakes have been masked out according to Tang et al., (2020).

References

Piecuch, C. G., & Ponte, R. M. (2011). Mechanisms of interannual steric sea level variability. *Geophysical Research Letters*, *38*(15). https://doi.org/10.1029/2011GL048440

Press, W. H. & Rybicki, G. B. (1989). Fast algorithm for spectral analysis of unevenly sampled data. *The Astrophysical Journal*, 338, 277–280.

Tang L., Li J., Chen J., Wang S.-Y., Wang R., Hu X. (2020). Seismic Impact of Large Earthquakes on Estimating Global Mean Ocean Mass Change from GRACE. *Remote Sens.* 12: (6) 935. https://doi.org/10.3390/rs12060935

VanderPlas, J., Connolly, A. Ivezic, Z. & Gray, A. (2012) Introduction to astroML: Machine learning for astrophysics. Proceedings of the Conference on Intelligent Data Understanding (2012)

VanderPlas, J. & Ivezic, Z. (2015) Periodograms for Multiband Astronomical Time Series. ApJ 812.1:18 (2015)

VanderPlas, J. *Understanding the Lomb-Scargle Periodogram* ApJS 236.1:16 (2018) https://ui.adsabs.harvard.edu/abs/2018ApJS..236…16V

Wessel, P., & Smith, W. H. F. (1996). A global, self-consistent, hierarchical, high-resolution shoreline database. *Journal of Geophysical Research: Solid Earth*, *101*(B4), 8741–8743. https://doi.org/10.1029/96JB00104